



AIAA 2002-1297

**INFLATABLE RIGIDIZABLE
ISOGRID BOOM DEVELOPMENT**

**John K. H. Lin, George H. Sapna III
David P. Cadogan, Stephen E. Scarborough
ILC Dover, Inc.
Frederica, DE**

**43rd AIAA/ASME/ASCE/AHS/ASC
Structures, Structural Dynamics, and Materials
Conference & Exhibit
AIAA Gossamer Spacecraft Forum
April 22-25, 2002 / Denver, CO**

**For permission to copy or republish, contact the copyright owner named on the first page.
For AIAA-held copyright, write to AIAA Permissions Department,
1801 Alexander Bell Drive, Suite 500, Reston, VA 20191-4344**

INFLATABLE RIGIDIZABLE ISOGRID BOOM DEVELOPMENT

John K. H. Lin^{*†}, George H. Sapna III^{*}, Stephen E. Scarborough^{*} and David P. Cadogan^{*‡}

ABSTRACT

Ultra-lightweight inflatable rigidizable space structures have been identified as an enabling technology for many large-scale and Gossamer type spacecraft planned by NASA and DoD for future space missions. The unique benefits of this class of structure, such as low packing volume, reduced complexity, and reduced mass, enable the development of large antennas, solar sails, and sunshields that would have been otherwise unrealizable. Through the maturation of this technology, many applications such as space based radar would benefit directly, and other applications such as mechanical actuation devices would benefit indirectly but significantly from material advancements.

ILC Dover, under contract to the Jet Propulsion Laboratory (JPL) and NASA Langley Research Center (LaRC), has developed an ultra-lightweight inflatable rigidizable boom structure for use on gossamer spacecraft.¹ The wall of the boom structural component is comprised of a grid-work of equilateral triangles that provide isotropic performance properties. This type of construction is termed an isogrid boom (See Figure 1). The grid-work is encased in two tubular polymeric films that act as gas containment vessels to enable inflation for deployment of the structure, and prevent the material from adhering to itself when packed. The exterior film also provides insulation to control the thermal conditions that govern the deployment process and structural performance in space. This structural concept was selected

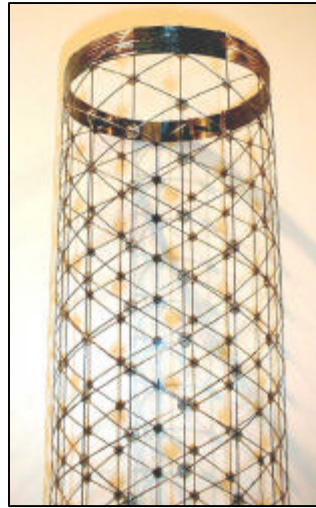


Figure 1. 24K Tow Inflatable Isogrid Boom without Membranes

for study because of its high structural efficiency and simplicity in design.

The material used in the fabrication of the isogrid structure is a composite, which consists of graphite and a shape memory polymer (GR/SMP). This GR/SMP material acts as a thermoplastic material and is able to be repeatedly heated and cooled to alter the structural shape. This allows the gossamer structure flight hardware to be packed and deployed for evaluation several times during ground test for checkout prior to launch and deployment in space. Shape memory polymers exhibit the unique property of returning to the originally formed shape when heated in a packed condition. In the case of structures with considerable deployment loads, inflation is used in conjunction with the weak SMP restoring force for deployment. This type of material was selected for study because of its structural performance properties, ability to be deployed and rigidized several times prior to launch, and storage life.

The overriding goal was to develop a structural rigidizable beam technology that was close to flight readiness. This goal was met by performing numerous materials development tests on several candidate composite materials, manufacturing and testing numerous sub-components and tube sections in simulated space and lab environments, and performing a deployment and rigidization test of a long boom section in a simulated space environment. The summation of the data indicated that the GR/SMP Isogrid was at a NASA Technology Readiness Level TRL of 5 to 6, but further study is required before the technology can be transitioned to a flight program.

INTRODUCTION

* ILC Dover, Inc., Frederica, DE

† Member AIAA

‡ Associate Fellow AIAA

ILC Dover Inc. has developed an ultra-lightweight isogrid structure that is manufactured from graphite unidirectional filaments coated with a high performance shape memory polymer resin. The work performed on this contract was conducted over the period of October 2000 to September 2001. Much of the foundation of the technology that was advanced in this effort was derived from work conducted by ILC on internal research and development programs. This work provided the necessary basis for development that allowed the effort to be completed within one year.

At the start of this program the Inflatable Solar Array Experiment (ISAE) application was baselined.² Soon afterward a more generic approach to mission application was taken. In addition to ISAE consideration, requirements from several planned gossamer spacecraft applications such as the New Millennium Program's ST6 Solar Array, the Large Radar Antenna program's mesh antenna support structure, and the Geostorm Warning program's solar sail support structure were used to develop a global requirements list for the technology. The various load regimes and performance needs yielded a bounded set of target values for development.

GOALS AND REQUIREMENTS

The inflatable isogrid development program began with a detailed requirement analysis of several applications (Geostorm Warning Solar Sails, Large Radar Antenna, NMP Solar Array, etc.) to identify specific structural and materials performance goals. A global system level requirements document was developed to establish goals for the design and development of the scalable inflatable isogrid composite tube for applications of Gossamer type structure. The inflatable isogrid requirements document consists of three sections: (1) the general design requirements, (2) the performance requirements, and (3) the environmental requirements.

General Design Requirements

- The stowage envelope of the inflatable isogrid composite structure shall be minimized.
- The mass of the inflatable isogrid composite structure shall be minimized. (Structural mass of 10 to 50 gm/m²)
- The stowed system shall be vented during ascent capable of withstanding maximum

pressure decay profile of 5240 Pa/sec [0.76 psi/sec] without auto-inflation.

- The design of the inflatable isogrid composite structure shall be capable of mass production.
- The accuracy (i.e. straightness and concentricity) of the inflatable isogrid composite tube shall be less than $a/L = 0.001$ as fabricated, where (a) is initial imperfection and (L) is the length of the structural boom or column.
- The deployed accuracy (i.e. straightness and concentricity) of the inflatable isogrid composite tube shall be less than $a/L = 0.005$, where (a) is imperfection after deployment in space and (L) is the length of the structural column as fabricated.

Performance Requirements

- The system level operational frequency shall be greater than 0.1 Hz.
- The system shall be capable of operating under combined acceleration of 0.015 g.
- The safety factor for structural elements of the inflatable isogrid composite structure shall be 1.25 for components qualified by static testing and 2.0 to yield and 2.6 to ultimate for components not qualified by static testing.
- The safety factor for inflatable structure shall be as follows:
- The relief pressure shall be designed to 1.5 times the operational pressure.
- The burst pressure shall be designed to 2.6 times the operational pressure.
- The inflatable isogrid composite structure shall be capable of multiple deployments (requirement = 5, goal = 20).
- The outgassing of the inflatable isogrid composite structure shall be less than 1% TML and less than 0.1% CVCM.
- The operational life of the inflatable isogrid composite structure shall be 8 years minimum.
- The stowage life of the inflatable isogrid composite structure shall be 2 years minimum.

Environmental Requirements

- The inflatable isogrid composite structure shall be capable of operating from LEO to deep space (5AU).
- The inflatable isogrid composite structure shall be capable of operating at

temperatures of ranging from -180°C to 50°C .

- The stowed inflatable isogrid composite structure shall be designed to survive the Shuttle launch environments without any damage.
- The requirements for ground environments shall be limited to less than launch environments.

DESIGN ANALYSIS

In the design and optimization of the isogrid boom structure several design parameters are important. These parameters are diameter of the tube, diameter of the tow, number of axial and helical tows that determine the rib spacing, the departure angle of the helical tow that determines the shape of the grid and the material properties of the rib structure. The isogrid structure developed in this effort was limited to a helical departure angle of 30° degrees (See Figure 2). This means that the intersecting ribs (i.e. axial and helical tows) of the grid form an array of equilateral triangles. This gave the boom isotropic properties. To reduce design and manufacturing variables, axial and helical tows were set to be identical in terms of number, diameter, and material throughout the entire length of the boom. For the purpose of structural model correlation, the parameters of tube diameter, the number of axial and helical tows, thus the rib spacing, and the structural material were fixed. The remaining parameter of tow diameter was limited to three different sizes that were selected based on fabrication and application considerations. In actual application, many of the above parameters could be varied in a single boom such as varying diameter in a tapered boom or varying the tow diameter to reinforce the structure locally. In addition to the consideration of design parameters, three failure mechanisms, namely overall Euler buckling of the column, local instability of the isogrid wall, and local rib buckling of the tow, were analyzed with pinned-pinned and fixed-free end conditions.

Structural Analysis

The analysis procedure presented in this section uses classical theory to analyze the structural performance of the isogrid wall tubular columns. Although in the design of grid structure there exist an infinite number of departure angles for the helical ribs with respect to the center axis of

the tube, the grid structure developed in this effort is limited to a helical departure angle of 30° degrees. In addition to fixing the rib orientation

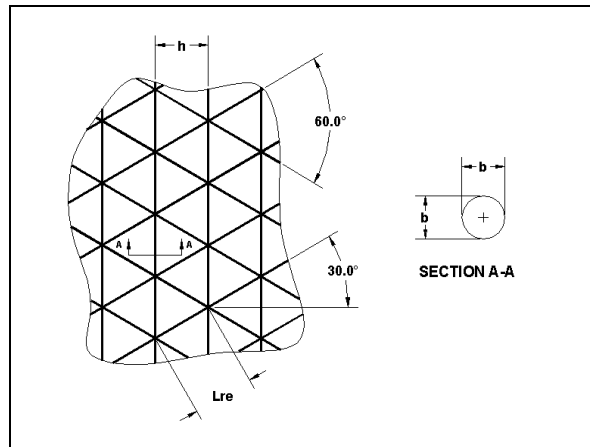


Figure 2. Isogrid Geometry

parameter, the tow or rib element cross section is assumed to be circular. Based on actual tow measurements conducted for this effort this assumption is nearly true. Therefore, it can be used without assuming an elliptical shape. Design procedures and equations are presented without lengthy derivation.

In the analysis of the isogrid structure, three modes of failure were considered: (1) the global Euler buckling of the column with both pristine (i.e. perfectly straight column) and imperfect (i.e. initially curved column) conditions, (2) the general instability of the tubular isogrid wall with manufacturing imperfection, and (3) the local Euler buckling of an individual rib element in the isogrid wall with both pristine and imperfect conditions. By taking imperfection into consideration, the procedure based on classical theory has been improved to provide fast solution that is closer to reality. At this point a word of caution is in order. The theory developed here assumed that the node or joint strength is greater than the lowest failure case presented above. However, this assumption is not always true. If the node failure is lower than the three modes of failure presented above it becomes a driving parameter.

The global Euler buckling equation of an isogrid tubular column with circular tows is derived by substituting the moment of inertia of the isogrid structure into the general column buckling equation.

$$P_E := \frac{C_k \cdot \pi^3 \cdot r^2 \cdot b^2 \cdot E \cdot n}{8 \cdot (L)^2} \quad \text{Equation (1)}$$

where (C_k) is the column end support coefficient. For example, (C_k) equals to 1.0 for column with simply supported ends. The moment of inertia for the isogrid tube is

$$I := \frac{\pi \cdot r^2 \cdot (b)^2 \cdot n}{8} \quad \text{Equation (2)}$$

To include the effects of initial imperfection and eccentric loading the following iterative equation is used to calculate a lower buckling load limit (P_L):

$$P_E := P_L \left[(1) + \frac{a \cdot A}{Z_s \left(1 - \frac{P_L}{P_E} \right)} + \frac{e \cdot c \cdot r}{(r_g)^2} \cdot \sec \left(\frac{\pi}{2} \cdot \sqrt{\frac{P_L}{P_E}} \right) \right]$$

Equation (3)

where (a) is the amplitude of imperfection; (e_c) is the eccentricity of axial compressive load; (r_g) is the radius of gyration; and (Z_s) is the section modulus.³

$$r_g := \sqrt{\frac{I}{A}} \quad Z_s := \frac{I}{r}$$

The equation for general instability is derived by substituting the stiffness of isogrid structure into the classical expressions for the isotropic monocoque shell structure. The equivalent isotropic Poisson's ratio (ν), extensional stiffness (C), and bending stiffness (D) for the isogrid structure with circular tows are as follows:

$$\nu := \frac{1}{3} \quad \text{Equation (4)}$$

$$C := \frac{9 \cdot \pi \cdot E \cdot (b)^2}{32 \cdot h} \quad \text{Equation (5)}$$

$$D := \frac{3 \cdot \pi \cdot E \cdot (b)^4}{128 \cdot h} \quad \text{Equation (6)}$$

where (b) is the diameter of the tows or rib elements and (h) is the distant between the axial tows. (h) can be expressed in terms of the number of axial tows (n) around the circumference and the radius (r) of the tubular column.

$$h := \frac{2 \cdot \pi \cdot r}{n} \quad \text{Equation (7)}$$

The equation for general instability (i.e. critical local buckling) of a cylindrical wall due to combined axial and bending loads with initial imperfection and eccentricity taken into consideration can be written as follows:

$$P_{CL} := 2 \cdot \pi \cdot r \cdot N_{CLC} - \frac{2 \cdot M_{ap}}{r} \cdot \left(\frac{N_{CLC}}{N_{CLM}} \right)$$

Equation (8)

where (N_{CLC}) is axial load per unit width of circumference for a cylindrical tube subjected to axial compression; (N_{CLM}) is axial load per unit width of circumference for a cylindrical tube subjected to maximum bending; and (M_{ap}) is the sum of bending moments due to combined axial and lateral loads.

where (M_L) is the maximum bending moment in the tube due to lateral loads or moments (such

$$N_{CLC} := \frac{P_{CLC}}{2 \cdot \pi \cdot r}$$

where,

$$P_{CLC} := c_2 \cdot 4 \cdot \pi \cdot \sqrt{C \cdot D \cdot (1 - \nu^2)} \quad \text{Equation (9)}$$

$$N_{CLM} := \frac{P_{CLM}}{2 \cdot \pi \cdot r}$$

where,

$$P_{CLM} := c_3 \cdot 4 \cdot \pi \cdot \sqrt{C \cdot D \cdot (1 - \nu^2)} \quad \text{Equation (10)}$$

$$M_{ap} := M_L + M_a \quad \text{Equation (11)}$$

as acceleration, gravity, other concentrated loads, or eccentric loads) and (M_a) is the maximum bending moment in the tube due to axial loads (such as axial compression or tension). In general, the applied moment is application and mission dependent and therefore must be solved in a case-by-case basis. The maximum bending moment due to axial compression load with imperfection and eccentricity taken into consideration can be written as

$$M_a := P \cdot \delta_t$$

where,

$$\delta_t := \delta_L \cdot K_c \quad \text{Equation (12)}$$

Here, (d_t) is the total lateral deflection of the column due to combined loads; (d_L) is the maximum lateral deflection without the axial compressive load; and (K_c) is the multiplication factor for calculating total deflection of a column when compressive load is added.⁴ Lateral deflection multiplication factor related to two applicable end support conditions have been derived and are presented as follows:

Case (1): Fixed-Free End Condition

$$K_c := \frac{\left(\frac{1 - k_1 L_1 \sin(k_1 L_1)}{\cos(k_1 L_1)} \right) \cos(k_1 x_1) + k_1 L_1 \sin(k_1 x_1) + \frac{(k_1 L_1 \sin(k_1 L_1) - 1)}{\cos(k_1 L_1)} + k^2 \left[\frac{(k_1^2)}{2} - L_1 x_1 \right]}{\frac{1}{8} (k_1 L_1)^4}$$

Equation (13)

Case (2): Pinned-Pinned End Condition

$$K_c := \frac{\left[1 - \cos(k_1 L_1) \right] \sin\left(\frac{k_1 L_1}{2}\right) - \left[(1) - \cos\left(\frac{k_1 L_1}{2}\right) + \frac{(k_1^2 L_1^2)}{8} \right] \sin(k_1 L_1)}{\frac{5}{384} (k_1 L_1)^4 \sin(k_1 L_1)}$$

Equation (14)

For both cases,

$$k := \sqrt{\frac{P}{E \cdot I}} \quad \text{Equation (15)}$$

The coefficients (c_2) and (c_3) in equations (9) and (10) are empirical correlation factors for isotropic shells under axial compression and

bending respectively to account for manufacturing imperfections.⁵

$$c_2 := 1 - 0.901 \cdot (1 - e^{-\phi}) \quad \text{Equation (16)}$$

$$c_3 := 1 - 0.731 \cdot (1 - e^{-\phi}) \quad \text{Equation (17)}$$

Where,

$$\phi := \frac{1}{16} \cdot \sqrt{\frac{r}{b}} \quad \text{for } r/b < 1500 \quad \text{Equation (18)}$$

The third mode of failure is the buckling of the axial rib element as a small Euler column.⁶ Assuming the rib element is a circular tow or rod, the familiar moment of inertia for a circular rod can be substituted into the standard Euler buckling formula to derive the rib buckling equation. Expressing in terms of the tube radius, rib diameter, and number of axial ribs, rib buckling of isogrid tube can be written as follows:

$$P_{RCR} := \frac{3 \cdot \pi \cdot c_1 \cdot E \cdot (b)^4 \cdot (n)^3}{1024 \cdot r^2} \quad \text{Equation (19)}$$

The coefficient (c_1) is the end fixity factor, which is assumed to be one (1.0). To include the effects of initial imperfection, the following iterative equation is used to calculate a lower rib buckling load limit (P_{LR}).

$$P_{RCR} := P_{LR} \left[(1) + \frac{a_r A_r}{Z_r \left(1 - \frac{P_{LR}}{P_{RCR}} \right)} \right]$$

Equation (20)

Where (a_r) is the initial imperfection in the rib; (A_r) is the area of the rib; and (Z_r) is the section modulus of the rib. This equation is important because rib imperfections will always occur to some extent.

$$Z_r := \frac{2 \cdot I_r}{b}$$

$$I_r := \frac{\pi \cdot b^4}{64}$$

$$A_r := \frac{\pi \cdot b^2}{4}$$

In this study the frequency of vibration for both a simply supported column and a fixed-free column are also calculated. For a simply supported column, the following equation is used.

$$f_{ss} := \frac{\pi}{2} \cdot \sqrt{\frac{E \cdot I}{M \cdot (L)^3}}$$

Equation (21)

For fixed-free column the following equation is used.

$$f_{ff} := \frac{1}{2 \cdot \pi} \cdot \sqrt{\frac{3 \cdot E \cdot I}{(0.236 \cdot M + m_t) \cdot (L)^3}}$$

Equation (22)

where (m_t) is the tip mass of the free end. The frequency equation for the fixed-free end condition is used for data correlation.

Finite Element Analysis

The finite element approach for the isogrid structural analysis assumed a structure of open cell boom comprised of graphite epoxy tows orientated in a circumferential isogrid. MSC/NASTRAN models were created for circular tubes of 17.78 cm [7.00 in] nominal diameter with various tow rib spacing, and boom lengths. The rib spacing parameter of the isogrid structure included four sizes of open cells ranging from 0.87 cm [0.344 in] to 4.65 cm [1.833 in] base length measured around the circumference of the tube. The length parameter, which included three different lengths of 0.322 m, 3.00 m and 7.00 m, were constructed based on the 0.322 meter model (See Figure 3). The length of the shortest model was determined based on the helix length of one helix segment. Material stiffness and strength properties were generated using composite

micromechanics and laminate code with tow diameter and fiber volume fraction as parametric variables. The parameter for the tow size varied from 3k to 48k by doubling the number of tows. The parameter for fiber volume fraction varied from 0.40 to 0.60 in 0.05 increments.

The result of the micromechanics analysis

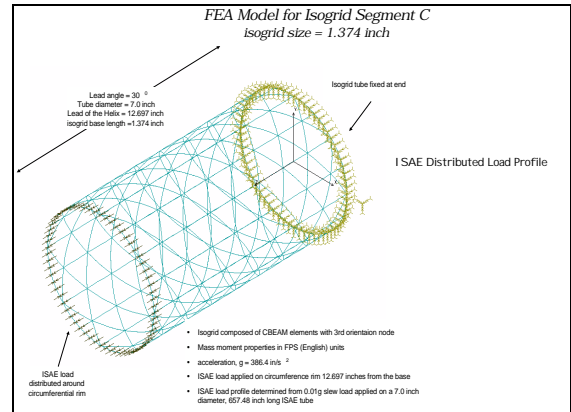


Figure 3. FEA Model of Isogrid Segment

indicated that longitudinal ultimate stress values are approximately 12 to 18 times greater than the transverse and shear ultimate stress values. Longitudinal ultimate stress values increase linearly with increasing tow fiber volume fraction from 0.40 to 0.60. Transverse and shear ultimate stress values are independent of tow fiber volume fraction. From the micromechanics analysis, one could conclude that tow structural performance is relatively insensitive to fiber volume fraction. Tows manufactured with a nominal 0.50 volume fraction will meet the structural performance requirements.

In the critical buckling analysis, critical buckling was compared to the Tsai-Hill failure criteria and Tai-Wu failure criteria for each value of fiber volume fraction. The failure criteria load factors calculated for all the tows showed a sufficient margin to conclude that the graphite/epoxy tows will deform without sustaining localized or catastrophic fracture under the applied load profile given above. The results also indicated that the cross sectional area of the tow is the governing parameter for determining the application of an isogrid boom.

Mass Analysis

The mass of the isogrid structure is calculated by

$$M_t := \gamma_n \cdot \rho \cdot L \cdot A \cdot \left[n_a + n_h \cdot \left(\frac{\sqrt{1 + \tan(\beta)^2}}{\tan(\beta)} \right) \right]$$

where

A = Area of the isogrid tow [$A = (\pi b^2)/4$]

b = Tow diameter of the isogrid tube

L = Length of the isogrid tube

n_a = Number of axial tows

n_h = Number of helical tows

β = Departure angle of the helical tow

γ_n = Empirical multiplication factor for the node reinforcements

ρ = Density of the composite material

This mass equation is a general equation applicable for different shape and number of tows and for different departure angle of helical tows.

ISOGRID STRUCTURE FABRICATION

Material performance of the GR/SMP used in the inflatable rigidizable isogrid boom is critical because of its effect on structural and thermal design. The current program concentrated its effort on the development of shape memory polymer composite materials. Data was generated for several materials through research including laboratory synthesis, compounding, resin characterization, and many standard material characterization tests. Testing included tensile, compression, coefficient of thermal expansion (CTE), flexibility, folding temperature, latency, outgassing, thermal conductivity, creep, and shape accuracy testing. Based on the results of the tests, the best GR/SMP candidate was selected to fabricate Developmental Verification Testing (DVT) units.

After material selection, DVT tubes were fabricated in one (1) meter long section to prove out fabrication processes, techniques, and structural designs. Based on the lessons learned from the DVT tubes, 18-cm diameter by 3-meter (See Figure 4)



Figure 4. Three Meter Isogrid Boom

and 7-meter long tubes were successfully fabricated.

Isogrid beams are manufactured using a modified thermoset filament winding process. Thermoset filament winding is a process that is widely used to make many axis-symmetric composite parts such as rocket motor cases, storage tanks, and pipes. It is a controlled technique of wrapping fiber rovings, or tows, around a mandrel, which has been formed to the shape of the final part. The fibers can either be coated with a specified amount of resin as they are wound around the mandrel (wet winding) or they can be pre-impregnated in an earlier process step and then wound around the mandrel (dry winding). ILC has selected a wet-winding process for this program because of its flexibility in allowing a number of manufacturing parameters to be readily altered for study.

STRUCTURAL TESTING

Structural testing was performed on numerous isogrid beam sections to characterize design performance, assist in manufacturing process enhancements, and provide data for analytical model correlation. This test program was broken down into two batteries of tests to isolate specific design parameters and to provide a cost-effective approach. DVT tubes (0.3m long by 0.18m diameter) were constructed and tested in compression and torsion to provide a rapid assessment of manufacturing methodologies and node strength. The length of the section was guided by the desire to test one complete "bay", which consisted of a spiral fiber wrap that traversed 360°, and the ability to test the article in the universal test machine (Instron). Twenty (20) DVT tubes with various node designs and tow diameters were fabricated and tested. First order packing effects were also studied in this battery of tests to study the effects of packing and deployment on node and element structural performance.

Long sections (3.0-m long by 0.18-m diameter) were constructed and tested in compression, torsion, bending, frequency, straightness accuracy, and length accuracy (See Figure 5). This battery of tests was

conducted on several beams in their as manufactured state, then after successive deployments (not to failure), and then to failure after a prescribed number of deployments. This allowed the cycle fatigue life of the booms to be studied and the degradation of the components to be assessed in a scenario that paralleled actual use of a flight system.

Data from all column testing was used to refine and correlate the analytical models that were developed for sizing the isogrid structures. Testing conducted on various sized tow bundles, 24K, 36K, and 48K, provided data that allowed scaling of the isogrid design to be studied.



Figure 5. 3m Boom Bending Testing at ILC

DATA CORRELATION

Compression Test Data Correlation

The compression tests performed in this development effort included short sections of DVT tubes and 3-meter long tubes. The tests were conducted with pinned-pinned end conditions. The results of the tests showed that the 18-cm diameter by 0.3-meter long tubes performed consistently better than the 3-meter long tubes. The average compressive peak load at break for the 0.3-meter tube is 500.00 N, which is 1.4 percent lower than the calculated result of 507.00 N. This comparison does not include packing effects. The average compressive peak load for the 3-meter long tubes is 421.00 N, which is 17 percent lower than the calculated result. Several factors could contribute to the lower compressive buckling load of the 3-meter tube in comparison with the 0.3-meter tube. First, the isogrid tube could be experiencing global Euler buckling behavior or reduced rib buckling earlier than predicted by the classical method. This could be due to an initial imperfection. Both modes of failure describe non-linear behavior. Second, the lower compressive load capability could be the result in initially curved axial ribs from CTE mismatch of the composite material and imperfections in the mandrel. Third, the lower compressive load capability could be the result of a manufacturing defect, such as a weak node reinforcement point. From testing observation and data

analysis, the following charts (Figure 6 and 7) were generated.

By analyzing the results of Figure 5, it is safe to conclude that the reduction of buckling load is not due to premature global Euler buckling behavior, because even with the imperfection taken into consideration the tubes are too short for Euler buckling behavior. However, when a global imperfection (i.e. curvature of the entire tube) is taken into consideration in the rib buckling behavior, a non-linear reduction in the rib buckling load is observed. With the ratio of imperfection, $a/L = 0.002$, which corresponds to approximately 6.00 mm of imperfection over a 3-meter long tube, calculated rib buckling is reduced from 507.00 N

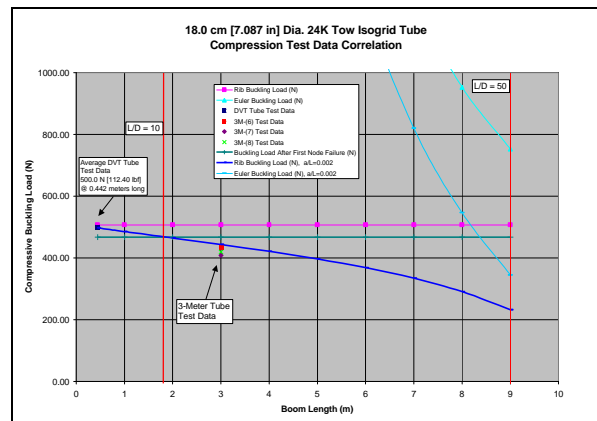


Figure 6. Compression Test Data Correlation Chart

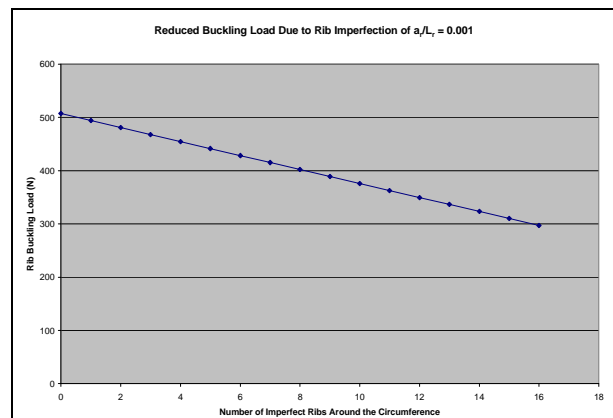


Figure 7. Reduced Rib Buckling Load Due to Rib Imperfection of $a_r/L_r = 0.001$

to 443.62 N. The new calculated solution for the 3-meter tube, with imperfection taken into consideration, is only 5.0 percent higher than the average 3-meter experimental result. If lower rib buckling load due to global imperfection is the cause of buckling capability reduction, then the results shows good correlation between the analytical solution and the experimental data. In fact, based on the straightness test results, this global imperfection in the order of the ratio mentioned above is observed. This outcome indicates that rib buckling due to global imperfection must be taken into consideration for long tubes prior to Euler buckling.

Figure 7, above, shows what happens to the rib buckling load as the number of imperfect ribs increases around the circumference of the tube. Based on the best design of 16 axial ribs, with an imperfection ratio of $a_r/L_r = 0.001$ (i.e. 0.035 mm imperfection over 35.0 mm rib length), as the number of imperfect ribs increased from zero to 16, the rib buckling load decreased from 507.00 N to 297.00 N. If 40 percent of the ribs (6 ribs) around a single circumferential section of the tube are imperfect by the above ratio the rib buckling load will reduce to 421.70 N. Although this cause is a possibility, it is not the most likely scenario.

Another possible cause of rib buckling load reduction is premature node failure. A single node failure in the isogrid tube can significantly reduce the rib buckling performance of the entire tube. This is apparent from the sudden increase in the effective length of a single rib, thus reducing the effective strength of that rib. To take this phenomenon into consideration, the original rib buckling equation was modified to simulate what happens when a single rib fails. Given the following parameters, rib buckling load after single node failure can be calculated as follows:

$$P_{RCRsnf} := \frac{3 \cdot \pi \cdot c_1 \cdot E \cdot b^4 \cdot n^2 \cdot (n - 1.25)}{1024r^2}$$

From the above calculation, one can observe that after a single node failure, rib buckling load reduces from 506.94 N to 467.34 N, which is a 7.8 percent reduction in strength. Based on the observation of 3-meter tube testing, which indicated failure consistently occurred first from node failure, it is safe to conclude that the

reduced buckling load is due to a combination premature node failure and global initial imperfection.

Data Correlation with FEA Model

To correlate the FEA model with structural properties data, the FEA model was exercised with identical end conditions and loads that were imposed during experimental testing. For the frequency analysis, the base of the column is fixed in translation for all degrees of freedom, and the tip is free. The tip mass, 1.2 kg, is equally distributed circumferentially around the top of the column. For the compression analysis, the 1.2 kg tip mass is replaced with a 4.448 N compressive force distributed circumferentially around the top of the column.

To identify the non-linear behavior of the isogrid tube, upper and lower bound material properties for the unidirectional tow were used in the FEA analyses. In other words, upper and lower bounded analyses are used to describe in linear analysis terms the performance of an inherently "non-linear," large length over diameter ratio tow segment in the isogrid structure. To generate these properties, micromechanics analysis was used to calculate a self-consistent material database to correlate with the experimentally measured tow modulus. Volume fraction of $V_f=0.455$ was used, which corresponds to the experimental 24k tow used in the 3-meter isogrid tubes.

From the results of the micromechanics analysis, three structural analytical FEA programs were used to calculate the bounded performance of the 3-meter tube. The results of all three solution methods, NE Nastran, MI Nastran, and Cosmos DesignStar, agree for frequency and Euler buckling. The results showed an average frequency of 3.45 Hz and an average buckling load of 439.46 N, which is in good agreement with experimental results (i.e. 3.33 Hz for frequency and 421.00 N for buckling load) based on the assumptions made for the material properties and the solution methods.

Bending Test Data Correlation

In the bending test, the 3-meter isogrid tubes were mounted in the three-meter test fixture with the base end caps bolted to the top of the fixture (in a clamped end condition) and the tip end caps unconstrained. Comparing the calculated solution with the test data of the baseline (no packing) tubes (See Figure 7), there was good

correlation (less than 10% difference) between the experimental results and the calculation method.

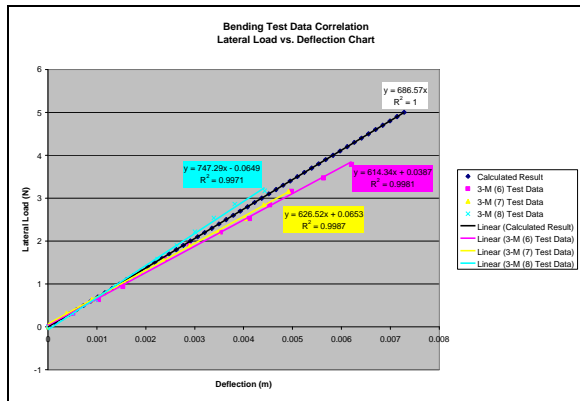


Figure 8. Bending Test Data Correlation

Frequency Test Data Correlation

The frequency test was conducted for the 3-meter long boom as a vertically mounted cantilever column with the base of the column secured to the concrete floor. The data presented showed that the frequency test yielded excellent results. The overall average frequency for this 3-meter long tube is 3.33 Hz with a standard deviation of 0.0393. Comparing the averages of test results with the analytical result shows a difference of 0.32 percent to 3.0 percent. Therefore, the analytical solution is in good agreement with the experimental results.

VACUUM CHAMBER TESTING

A thermal-vacuum chamber deployment test of a 3-meter isogrid composite tube was successfully conducted at NASA Langley Research Center. The test was carried out in the 8x15 vacuum chamber located in Building 1250 of NASA LaRC. The test article was a 3-meter isogrid boom constructed of 24K wound carbon fibers and TP283E resin. The boom assembly, mounted inside the heater box, was in the stowed configuration when it was installed into the chamber (See Figure 9). The entire assembly was mounted to one end of the chamber allowing the boom to deploy horizontally toward the other end. After installation and inspection of all connections, the chamber was closed and then pumped down. Once the chamber reached the desired pressure, the chamber shroud was cooled by nitrogen to the test temperature of -180°C. At the same time the shroud is being cooled, the

heater box was powered to heat the packed boom to the required deployment temperature of 80°C. When all thermocouples inside the

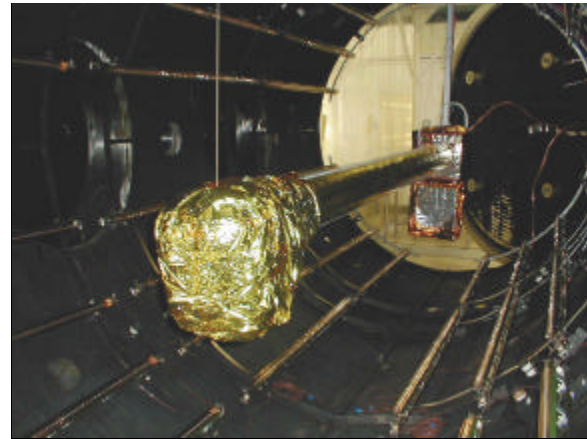


Figure 9. Thermal Vacuum Chamber Test Article Fully Deployed

packed boom reached the required deployment temperature, the boom was deployed via inflation gas. Throughout the entire experiment, temperature and pressure of the chamber and the test article were monitored and recorded.

During the experiment two unexpected events occurred. First, the time to heat the packed assembly to deployment temperature was much longer than the predicted by the thermal model. This difference between the model and the test could be attributed to the incorrect assumption of e^* values for the tip MLI oven and the MLI of the heater box due to assumptions that were made about the amount of compression on the stack and the bulk contact conductance. Second, the deployment time of 2 minutes was not maintained due to a problem with the inflation system. The entire deployment, with limited control, took less than 10 seconds. This anomaly was caused by residual gas at atmospheric pressure in the line between the pressure regulator and the needle control valve. To eliminate this problem in the future, line gas before the needle control valve and pressure regulator must be purged to vacuum before switching the inflation line to deploy the boom. Despite the two unexpected events, the experiment was a success in that it proved the feasibility of the design.

SUMMARY

The work conducted in the GR/SMP Isogrid development program demonstrates the efficacy of using the graphite/shape memory polymer

composite isogrid structure in high performance, high packaging efficiency spacecraft structures. The GR/SMP isogrid structure provides a low mass alternative to current state-of-the-art mechanically deployable structures to facilitate the construction and launch of space structures with a high packed to deployed volume ratio such as antennas, solar sails, telescopes and sunshields.

The GR/SMP isogrid program advanced the state-of-the-art. Several materials have been developed that demonstrate low outgassing, high strength and stiffness, as well as the ability to be packed and deployed without appreciable damage. Design and manufacturing techniques have been developed for ultra-lightweight isogrid structures that demonstrate resilience under load and meet design needs, and analytical models have been developed and correlated with test data. The result is that the technical maturity of the GR/SMP isogrid structure reached a TRL of 5 to 6.

ACKNOWLEDGEMENT

During this project ILC worked closely with the program's Technical Monitor, Ms. Jessica Woods-Vedeler, NASA Langley's vacuum chamber staff and other technical staff at NASA Langley Research Center such as Ms. Judith Watson (structural testing), and program technical consultants Dr. Martin Mikulas, to meet the goals of the program. The authors thank NASA and JPL for funding this effort. The authors especially thank Ms. Jessica Woods-Vedeler for her support.

REFERENCE

1. Cadogan, D., Lin, J., Sapna, G., Scarborough, S., "Space Inflatable Technology Development for Solar Sails and Other Gossamer Applications: GR/SMP Isogrid Boom Development Final Report," NASA Task Order 10442, ILC Dover, Inc., October, 2001.
2. Cadogan D., Lin J., *Inflatable Solar Array Technology*, 37th AIAA Aerospace Sciences Meeting and Exhibit, 1999.
3. Ugural, A.C. and Fenster S.K., *Advanced Strength and Applied Elasticity*, Elsevier Science Publishing Co., Inc., New York, NY, 1975.
4. Venkatraman, B. and Patel, S. A., *Structural Mechanics with Introduction to Elasticity and Plasticity*, McGraw-Hill, Inc., New York, NY, 1970.
5. Anon. NASA Space Vehicle Design Criteria: *Buckling of Thin-Walled Circular Cylinders*, NASA SP-8007, 8/1968.
6. Mikulas, Martin M., Jr., *Structural Efficiency of Long Lightly Loaded Truss and Isogrid Columns for Space Applications*, NASA Technical Memorandum 78687, NASA Langley Research Center, Hampton, Virginia, 7/1978.
7. Cadogan D.P., Selected chapters, *Gossamer Spacecraft: Membrane and Inflatable Structures Technology for Space Applications*, ISBN 1-56347-403-4 , Copyright: March 2001.
8. Cadogan D.P., Scarborough, S.E., *Rigidizable Materials for use in Gossamer Space Inflatable Structures* (AIAA 2001-1417), 42nd AIAA/ASME/ASCE/AHS/ASC SDM Conference, 2001.
9. Cadogan D., Lin J., Grahne M., *The Development of Inflatable Space Radar Reflectarrays* (AIAA 99-1517), 40th AIAA/ASME/ASCE/AHS/ASC SDM Conference, 1999.
10. Cadogan D., Lin J., J. Huang, A. Ferial., *An Inflatable Microstrip Reflectarray Concept for Ka-Band Applications*, 41st AIAA/ASME/ASCE/AHS/ASC SDM Conference, 2000.
11. Darooka D.K., Cadogan D.P., Scarborough S.E., *An Evaluation of an Inflatable Truss Frame for Space Applications* (AIAA 2001-1614), 42nd AIAA/ASME/ASCE/AHS/ASC SDM Conference, 2001.
12. Mikulas, Martin, "Structural and Micromechanics Aspects of Rigidizable Structures," University of Colorado Presentation, July 2000.